Journal of Energy Storage 145 (2026) 119910

Contents lists available at ScienceDirect

Journal of Energy Storage

journal homepage: www.elsevier.com/locate/est

Review article

Power hardware in the loop-based lifetime assessment of hybrid energy storage systems: A novel realistic approach

Seyede Masoome Maroufi [a,*], Dario Pelosi [b], Linda Barelli [b], Giovanni De Carne [a]

[a] Institute for Technical Physics, Karlsruhe Institute of Technology (KIT), Hermann-von-Helmholtz Platz 1, 76344 Eggenstein-Leopoldshafen, Germany
[b] Department of Engineering, University of Perugia, Via G. Duranti, 93, 06125, Perugia, Italy

ARTICLE INFO

Keywords:
Hybrid Energy Storage Systems
Flywheel energy storage systems
Frequency control
Power Hardware-in-the-Loop

ABSTRACT

Reliable and cost-effective energy storage is essential for grid applications, but lithium-ion batteries face lifetime limitations due to cycling stress, temperature effects, and high power ramping. This paper presents a novel Power Hardware-in-the-Loop (PHIL) approach for experimentally assessing battery aging in Hybrid Energy Storage Systems (HESS) that combine batteries with flywheels. The proposed setup enables realistic emulation of field conditions and long-term degradation testing. Two configurations are experimentally evaluated: a standalone battery system and a hybrid flywheel–battery system with equivalent energy capacity. Results show that the HESS configuration significantly reduces power ramping and depth of discharge, resulting in lower degradation rates than a standalone battery. Furthermore, a Levelized Cost of Storage (LCOS) analysis confirms that the HESS achieves superior lifetime economics under realistic operating conditions, particularly under end-of-life criteria.

Contents

* Corresponding author.
E-mail addresses: seyede.maroufi@kit.edu (S.M. Maroufi), dario.pelosi@unipg.it (D. Pelosi), linda.barelli@unipg.it (L. Barelli), giovanni.carne@kit.edu (G.D. Carne).

https://doi.org/10.1016/j.est.2025.119910
Received 3 August 2025; Received in revised form 13 November 2025; Accepted 12 December 2025
Available online 19 December 2025
2352-152X/© 2025 The Authors. Published by Elsevier Ltd. This is an open access article under the CC BY license (http://creativecommons.org/licenses/by/4.0/).

1. Introduction

The increasing deployment of Battery Energy Storage Systems (BESS) in grid applications has highlighted their crucial role in enabling renewable integration, stabilizing power fluctuations, and supporting grid resilience [1,2]. However, BESS faces significant challenges, primarily due to cycling degradation, capacity fade, and high replacement costs, which hinder its long-term economic viability [3]. As demand for energy storage solutions grows, there is a pressing need for improved strategies to enhance battery lifespan and efficiency.

Hybrid Energy Storage Systems (HESS), which integrate BESS with complementary power-intensive storage technologies such as Flywheel Energy Storage Systems (FESS) and Supercapacitor Energy Storage Systems (SCES), have emerged as a promising solution [4,5]. By leveraging the strengths of both energy-intensive and power-intensive storage devices, HESS can reduce battery cycling stress, improve response time, and optimize energy dispatch [6–8] . Despite these advantages, the adoption of HESS remains limited due to the absence of standardized sizing, control, and validation approaches. Existing studies predominantly rely on theoretical simulations and lack experimental validation under realistic grid conditions, making it difficult to quantify the actual benefits of HESS implementations [9–11].

In this study, a FESS is adopted as the power-dense component of the HESS due to its high power capability, ability to handle rapid charge–discharge events with minimal degradation, together with long cycle life and high efficiency. The flywheel's mechanical structure enables efficient mitigation of short-term power fluctuations while maintaining stability during repetitive operation, making it well-suited for the Power Hardware-in-the-Loop (PHIL) setup used in this work [12]. In future research, the same experimental framework will be extended to a SCES to investigate its influence on dynamic performance and the lifetime of both lithium-ion and sodium-ion batteries.

On the other hand, battery aging remains a critical concern in energy storage systems, particularly for lithium-ion technologies used in HESS. While numerous studies have modeled battery degradation under idealized conditions, there is a notable scarcity of realistic experimental investigations that account for the operational dynamics of hybrid configurations. Most aging analyses are performed either in steady-state cycling regimes or with simplified load profiles, which fail to reflect the rapid power fluctuations and irregular usage patterns typical of HESS applications [13–15]. As a result, the impact of hybridization on extending battery life and reducing degradation remains insufficiently understood. There is a clear need for comprehensive experimental methodologies that can capture real-world stressors, validate aging behavior under hybrid operation, and support more accurate predictions of long-term performance and costs.

This study addresses these challenges by introducing an experimental validation approach that integrates PHIL testing at a relevant scale with accelerated aging experiments at the single-cell level. Unlike conventional simulation-based evaluations, PHIL provides a realistic dynamic testing environment, capturing the complexities of grid interaction and HESS performance. By coupling PHIL with battery aging assessments, this work evaluates HESS effectiveness in mitigating battery degradation.

The experimental case study focuses on a microgrid scenario that delivers primary frequency regulation, where the HESS manages power variations originating from fluctuating load and renewable generation profiles. The power profile shown in Fig. 1 used for the tests is derived from previous studies and represents the dynamic requirements of primary frequency control [16,17]. Furthermore, the levelized cost of Storage (LCOS) is analyzed for both standalone BESS and HESS configurations, based on the outcomes of the combined PHIL and aging experiments.

The main innovations can be summarized as follows:

- A novel PHIL-based experimental setup that realistically emulates FESS operation under grid-relevant dynamics.
- Integration of PHIL experimental results with laboratory battery aging tests.
- Comparative lifetime and economic analysis (LCOS) between standalone BESS and hybrid FESS–BESS configurations, under identical power conditions.

This paper is structured as follows. Section 2 presents the methodology, detailing how PHIL testing is combined with battery aging experiments to evaluate HESS performance. Section 3 provides an overview of the modeling approaches used for the two Energy Storage Systems (ESS) within the HESS architecture. Section 4 describes the power management strategy employed to coordinate the operation of the two ESS. The experimental results are discussed in Section 5, followed by a techno-economic analysis based on the LCOS in Section 6. Finally, Section 7 summarizes the key findings and implications of the study.

2. Power hardware in the loop-based aging approach

Battery aging is estimated through a methodology that combines accelerated aging tests and dynamic simulations. These tests are based on the state of charge (SoC) evolution of a Li-ion battery, derived from a dynamic model of an ESS developed to manage power profiles for frequency regulation in the micro-grid.

The methodology enables a comparative lifespan assessment of the battery under two configurations:

- **Case 1:** A Hybrid Energy Storage System (HESS) consisting of a Li-ion battery and a flywheel.
- **Case 2:** A stand-alone Li-ion battery system with capacity equivalent to the battery in Case 1.

To ensure accuracy, the HESS model in Case 1 is refined via PHIL testing, particularly for the flywheel. Once validated, this model is used to simulate the SoC profile of the battery under realistic operating conditions. These simulations support aging tests to assess battery lifespan in both configurations.

A detailed model of the micro-grid, including the HESS for Case 1, is implemented in MATLAB/Simulink. The real power profile shown in Fig. 2, is managed using a Simultaneous Perturbation Stochastic Approximation (SPSA) algorithm, which dynamically allocates power between the battery and flywheel based on their operating C-rates, efficiencies, and SoC levels, in line with a multi-objective power management function.

For Case 2, the model is adjusted by removing the flywheel and allowing the battery to manage the entire power profile. This comparative setup allows evaluation of how HESS integration impacts battery cycling and aging. The study ultimately aims to quantify the potential lifespan extension achieved by coupling a Li-ion battery with a power-intensive device such as a flywheel (see Fig. 2).

Further details on the PHIL setup and aging mechanisms are provided in the following subsections.

2.1. Power hardware in the loop experimental setup

PHIL setup enables real-time interaction between simulations and physical hardware, allowing for a realistic evaluation of HESS performance under grid fluctuations and transient power demands. As shown in Fig. 3, the PHIL framework consists of: (1) a real-time simulation environment, where the control algorithms for HESS are implemented using the Opal-RT OP5700 real-time simulator; (2) an actual hardware setup, including a 120 kW, 8 kWh FESS (technical features are summarized with the specification in Table 1 that interacts with the simulated power system; and (3) a power amplifier group (Egston GAMP6, 2x200 kVA), which ensures accurate power flow between the simulated and physical components.

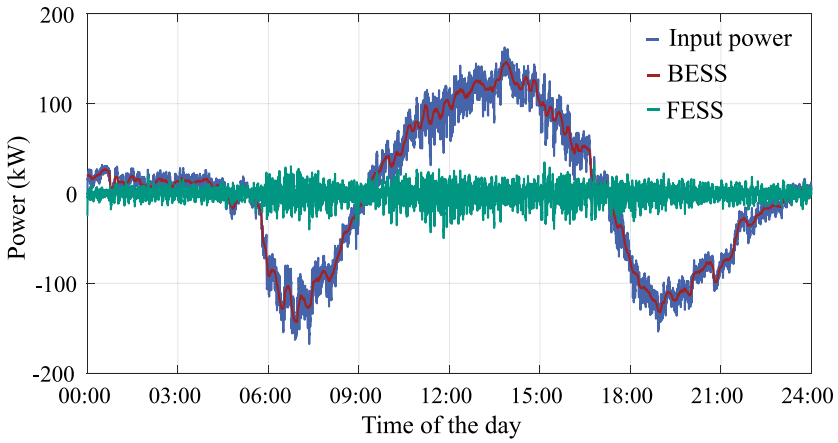

Fig. 1. The profile of the input power, battery power, and flywheel power [17].

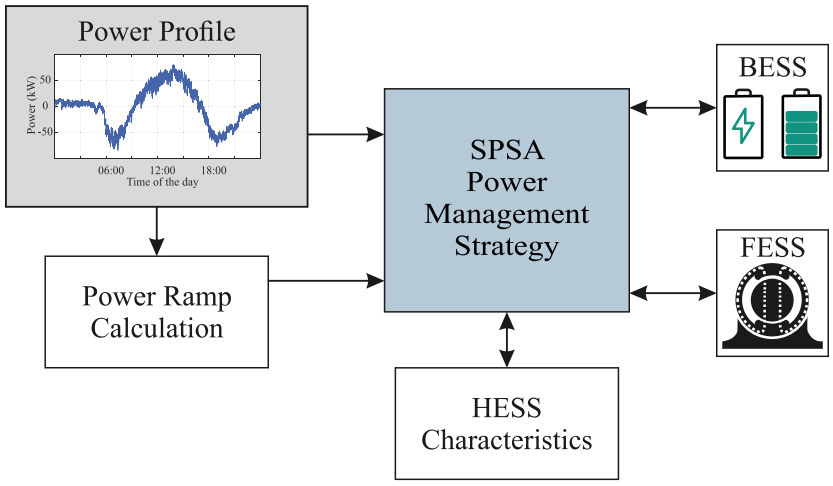

Fig. 2. Schematic of the micro-grid dynamic model integrating HESS (Case 1).

Table 1
Flywheel energy storage parameters.

Parameter	Value
Nominal power	120 kW
Nominal energy	8 kWh
Max current	160 A
AC voltage	400 V
DC voltage	720 V
Max cooling power	16 kW
Max speed	750 Hz

The SPSA-based power management strategy explained in Section 4.1 optimizes the power split between the flywheel and battery, prioritizing rapid fluctuations for the flywheel and smoothing battery input power. The SPSA algorithm provides the optimal power share in terms of two coefficients: q_{BESS} and q_{FESS}, representing the proportion of the total input power allocated to the battery and flywheel, respectively. These coefficients are then further adjusted using a control parameter that accounts for the SoC and power constraints of both energy storage systems. Based on this adjustment, the final reference power for each storage unit is determined.

2.2. BESS aging experimental setup

To assess the impact of HESS on battery lifespan, we conduct accelerated aging experiments on two Samsung INR18650-20R lithium-ion cells. The test setup includes a NEWARE BTS4000-5V20 A galvanostat/potentiostat system, which controls charge–discharge cycles and monitors cell performance over time. Cell specifications are deduced from the manufacturer's datasheet [18].

Cells were cycled within an operating voltage range of 2.5–4.2 V, with maximum continuous charge and discharge currents of 4 A and 20 A, respectively. This was done while considering the maximum allowable current range of the battery testing system. During the experimental activity, cells were maintained at a fixed temperature of 20±1 °C. This temperature setting was selected to replicate the controlled environment of stationary battery racks used in microgrid frequency regulation applications, where climate systems typically maintain temperatures within a narrow range (approximately 18–21 °C) [19]. Such limited variations have a negligible influence on battery performance; therefore, 20 °C was chosen as a representative setpoint for consistent comparison. Fig. 4 illustrates the described experimental test rig.

Aging estimation follows a three-step process:

1. ESS Modeling & Simulation: The HESS model is refined using PHIL data to generate realistic SoC evolution profiles.

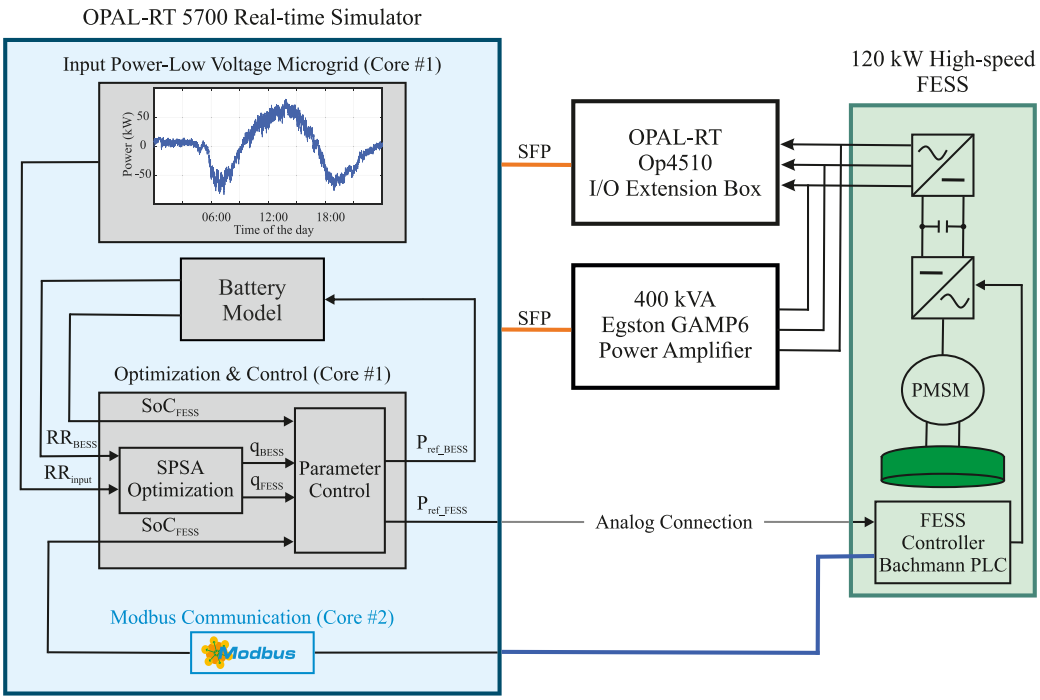

Fig. 3. Power hardware in the loop setup.

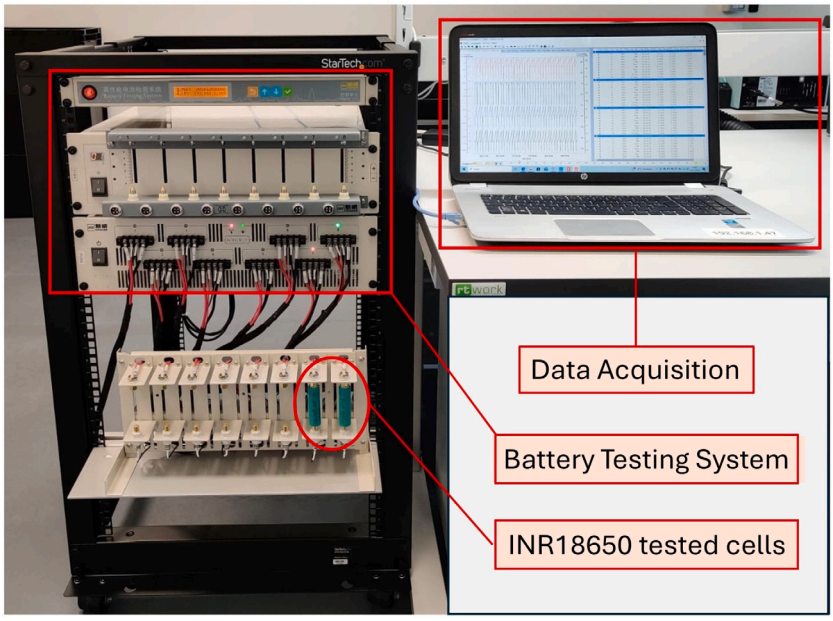

Fig. 4. Experimental test rig for aging tests on Li-ion cells.

2. Rainflow Cycle Counting (RFC): SoC profiles are processed to extract charge–discharge cycles categorized by depth-of-discharge (DoD).
3. Accelerated Aging Tests: Experimental tests replicate the extracted cycle profiles, allowing for direct comparison of battery degradation in standalone BESS and HESS configurations.

By integrating PHIL results with RFC analysis and accelerated aging tests, this method provides a realistic battery lifespan assessment, capturing both control strategy effects and real-world cycling behavior. The complete methodology is summarized in the flowchart in Fig. 5, illustrating the integration of PHIL data, RFC analysis, and accelerated aging tests for a comprehensive battery lifespan assessment.

3. BESS and FESS modeling

The Li-ion battery model follows an equivalent circuit approach, incorporating open-circuit voltage (V_{bat}), internal resistance (R_{bat}^{int}), and charge/discharge efficiency (η). Battery current and voltage are determined based on power demand, with V_{ocv} and R_{bat}^{int} obtained from experimental look-up tables. The SoC evolves as:

$$SOC_{bat}(t) = SOC_{bat} - (t-1)\int \frac{\eta I_{bat}}{Q}\, dt \tag{1}$$

where Q is the nominal battery capacity. The charge/ discharge efficiency accounts for internal resistance losses, ensuring accurate energy balance estimation.

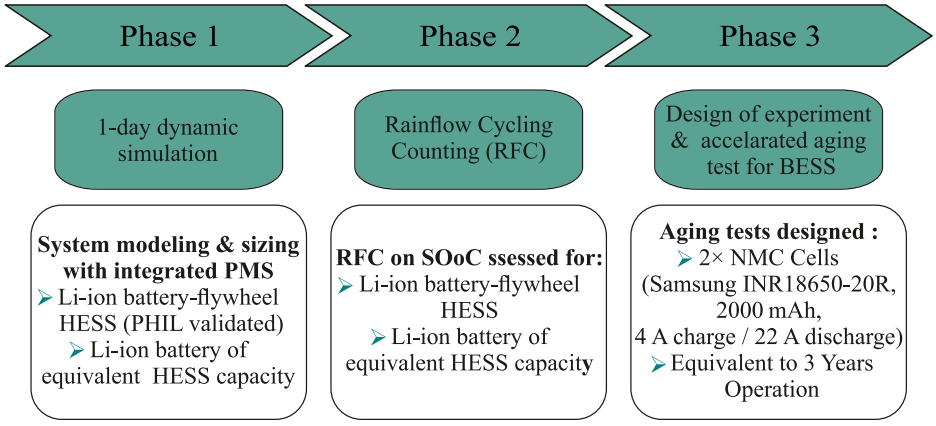

Fig. 5. Schematic flow chart of the developed methodology.

The FESS is modeled as a kinetic energy storage device, responding rapidly to peak demands and reducing stress on the battery. Its power exchange is expressed as:

$$P_{\text{FESS}}(t) = T\omega(t) + P_{\text{loss}}(t) \tag{2}$$

where T is the shaft torque, ω is the angular velocity, and P_{loss} represents friction and aerodynamic losses.

The FESS model is calibrated using PHIL experiments, ensuring accurate emulation of real-time performance. Specifically, loss parameters are tuned based on the installed 120 kW, 7.6 kWh flywheel (STORNETIC) at KIT to reflect real-world efficiency under frequency regulation conditions.

4. Power management strategy: Problem formulation

Power management strategy is developed based on SPSA algorithm, which theory is described in Section 4.1. Concerning the problem formulation designed for micro-grid frequency support, the input power to be managed has to be instantaneously split between the flywheel and the battery. Therefore, the vector of unknown parameters (θ) is defined as three dimensionless shares (i.e., Li-ion battery, flywheel, and grid, namely q_{BATT}, q_{FW}, and q_{GRID}), expressed by (3). It is highlighted that q_{GRID} share is included to consider a residual power not managed by the HESS.

$$\theta = \begin{bmatrix} q_{\text{BATT}} \\ q_{\text{FW}} \\ q_{\text{GRID}} \end{bmatrix} \tag{3}$$

Consequently, the split power values are calculated according to (4):

$$\begin{cases} P_{\text{BATT}} = q_{\text{BATT}}\,\Delta P \\ P_{\text{FW}} = q_{\text{FW}}\,\Delta P \\ P_{\text{GRID}} = q_{\text{GRID}}\,\Delta P \end{cases} \tag{4}$$

Where $\Delta P = P^{t}_{\text{freq}} - P^{t-1}_{\text{GRID}}$ (W) is defined as the difference between the required power for frequency regulation at time t and the residual power at the previous instant $(t-1)$. The SPSA parameters, detailed in Section 4.1, are selected according to previous research [20]. The power shares instantaneously assigned must pursue the following objectives:

I. Maximize micro-grid frequency support, minimizing residual power not managed by HESS over the day within the micro-grid as detailed in:

$$y^{t}_{1}(\theta) = \left(\frac{q_{\text{GRID}}\Delta P}{1000}\right)^{2} \tag{5}$$

II. Smooth the Li-ion battery power profile by means of the ratio between the battery power at timestep t and at the previous instant $(t-1)$, as expressed by:

$$y^{t}_{2}(\theta) = \left(\frac{q_{\text{BATT}}\Delta P}{P^{t-1}_{\text{BATT}}}\right)^{2} \tag{6}$$

The multi-objective problem is therefore modeled by means of the weighted sum of the objectives expressed by (5) and (6), defining the SPSA loss function as (7):

$$y^{t}(\theta) = w_1 y^{t}_{1}(\theta) + w_2 y^{t}_{2}(\theta) \tag{7}$$

Where the two weights w_1 and w_2 are both set at 0.5. The iterative process starts based on the initial estimate of the vector θ, as specified by (8):

$$\theta = \begin{bmatrix} 0.2 \\ 0.78 \\ 0.02 \end{bmatrix} \tag{8}$$

4.1. Stochastic power management strategy: Theory and implementation

Managing non-programmable power generation is increasingly complex, requiring efficient real-time power sharing among renewable sources, hybrid energy storage, and the grid. Optimization algorithms like linear, non-linear, dynamic, stochastic, and AI-based methods aim to minimize objectives such as emissions or costs [21,22]. However, AI faces challenges like convergence issues and dependence on initial estimates.

Multivariate stochastic optimization, particularly gradient-based algorithms like SPSA and Lyapunov, is effective for real-time power management, requiring no future knowledge or mathematical models [23]. SPSA, introduced in 1992 and further developed by [20,24], is a fast convergent solution for global optimization with advantages like no need for gradient information, lower computational load, and robustness to noise [25–29].

SPSA works by iteratively perturbing the parameters vector ($\hat{\theta}$) and updating it using the Eqs. (9)–(10), with parameters selected to ensure convergence [20,21]. In each iteration, the vector $\hat{\theta}$ is updated by perturbing its current estimate, as shown in (11), and the loss function gradient is approximated by (12). The estimate is updated with (13), continuing until the maximum iterations or convergence is reached.

$$a_k = \frac{a}{(A+k+1)^{\alpha}} \tag{9}$$

$$c_k = \frac{c}{(k+1)^{\gamma}} \tag{10}$$

$$\hat{\theta}^{\pm}_{k} = \hat{\theta} \pm c_k \Delta_k \tag{11}$$

$$\hat{g}_k(\hat{\theta}_k) = \frac{\partial L_k}{\partial \theta_k} = \frac{y(\hat{\theta}_k^+) - y(\hat{\theta}_k^-)}{2c_k} \begin{bmatrix} \Delta_{k1}^{-1} \\ \Delta_{k2}^{-1} \\ \vdots \\ \Delta_{kp}^{-1} \end{bmatrix} \tag{12}$$

$$\hat{\theta}_{k+1} = \hat{\theta}_k - a_k \hat{g}_k(\hat{\theta}_k) \tag{13}$$

The iterative process terminates once either the maximum number of iterations or the convergence condition is reached.

4.2. Rainflow Cycle Counting

Rainflow Cycle Counting (RFC) is a common algorithm used to assess fatigue stress on materials by counting cycles and analyzing their depths, which helps estimate failure cycles based on cycle amplitude [30]. RFC has also been applied to electrochemical devices, such as batteries, to evaluate their lifespan under complex charging/discharging cycles [23,27,31–33]. RFC identifies cycles from local extrema in the load profile, with the load being the battery's SoC variation. The SoC-time curve is rotated 90° clockwise, and the time axis is inverted [34,35]. RFC identifies local minima and maxima in the SoC as reversals, resembling water droplets on a roof.

According to the ASTM standard [36], the RFC procedure includes:

I. Counting half-cycles, ending when:
   - The time history ends.
   - Merging with an earlier reversal.
   - Encountering a larger magnitude trough.

II. Assigning a magnitude to each half-cycle as the stress difference between its start and termination.

III. Pairing half-cycles of equal magnitude in opposite directions to determine full charge–discharge cycles. For lithium-ion batteries, only cycles with a DoD greater than 2% are considered [37].

In this work, RFC was applied to the simulated SoC profiles of the battery under both standalone BESS and HESS configurations. The algorithm decomposes the SoC variations into individual charge–discharge cycles, categorized by their DoD. This classification enables a more detailed understanding of the cycling patterns experienced by the battery and their impact on aging. By analyzing the frequency and amplitude of these cycles, a representative charge–discharge profile was constructed. This information served as the basis for designing accelerated aging tests that emulate the real-world cycling behavior of the battery.

5. Results and discussion

In the following subsections, the experimental validation and results are described in detail.

5.1. HESS performance evaluation and RFC analysis

The FESS acts as the power-intensive component in the HESS, rapidly absorbing and delivering power to smooth fluctuations in the load profile. This capability alleviates the stress on the Li-ion BESS, enhancing its lifetime. To evaluate this effect, simulations and PHIL experiments were conducted.

Three representative 30-minute power windows—(i) maximum mean power, (ii) minimum mean power, and (iii) power crossing zero—were selected from the daily input profile shown in Fig. 6. The simulated power shares between FESS and BESS were applied to the PHIL system, enabling real-time validation. The measured FESS output was used to calibrate the modeled losses, which averaged around 2 kW (ranging from 1.5 to 2.2 kW), with a final SoC discrepancy below 1.7 percentage points. Table 2 reports the power loss values obtained from the fine-tuning of the FESS model by means of PHIL tests

Table 2
Assessment of FESS power losses to emulate real FESS behavior.

Case	$P_{loss}(kW)$	$SoC_{fin}(\%)$	$SoC_{fin}(\%)$
Pattern 1	2.2	50.3	49
Pattern 2	1.5	57.1	55.5
Pattern 3	2.2	51.7	51.45
Average	2		

The calibrated FESS model was then integrated into the HESS dynamic simulation. Results show that the BESS capacity required in Case 1 (with HESS) is 876 kWh, compared to 884 kWh in Case 2 (standalone BESS), as shown in Table 3. In addition to this capacity reduction, the power profile of the BESS in Case 1 was significantly smoother due to the peak shaving effect of FESS. This is further confirmed by the cumulative density functions (CDFs) of power ramps (Fig. 7(a)), where the ramp rate is limited to 0.5 kW/s in Case 1, compared to 1.8 kW/s in Case 2. Moreover, daily residual power not managed by the HESS remains under 6 kWh (Fig. 7(b)).

5.1.1. RFC-based stress analysis

To quantitatively assess battery stress, RFC was applied to the simulated SoC profiles of both Case 1 and Case 2. The resulting cycles, shown in Table 4, demonstrate that the HESS (Case 1) experiences shallower DoD cycles and a higher minimum SoC (19%) compared to Case 2 (12.1%). These results, visible in the daily SoC trends (Fig. 8), confirm that FESS operation reduces cycling severity and improves battery utilization. Case 2 is characterized by deeper and more pronounced SoC excursions, underscoring the effectiveness of FESS in reducing battery stress.

5.2. Accelerated aging tests and results

The RFC-based cycling profiles were used to design an accelerated aging test campaign on Samsung SDI INR18650-20R cells, following the conditions outlined in Section 4.2. Each RFC-identified cycle was scaled in current to match maximum continuous values, reducing test duration to about 16–17 days per equivalent year. Table 5 summarizes the step cycles used.

After three equivalent years of cycling, experimental results show that the cell in Case 1 retained 1501.7 mAh, while the one in Case 2 dropped to 1302.9 mAh, as reported in Table 6. This corresponds to SoH values of 75% and 65%, respectively (Fig. 9(a)). These findings highlight the clear benefit of HESS integration in reducing degradation and extending the usable life of the battery.

6. Techno-economic impact of HESS on battery performance

The experimental results confirm that integrating a FESS with a BESS in a HESS configuration significantly improves system performance. The HESS setup reduces high-frequency power fluctuations, leading to smoother battery operation and lower DoD cycles. The RFC analysis revealed that HESS reduces large amplitude charge–discharge cycles, a major contributor to battery degradation.

These findings align with previous studies on hybrid storage systems, where high-power energy storage devices, such as supercapacitors and flywheels, reduce BESS cycling stress. However, unlike many prior studies that rely solely on simulations, this study validates HESS performance through PHIL testing, ensuring that real-world dynamics and efficiency losses are considered.

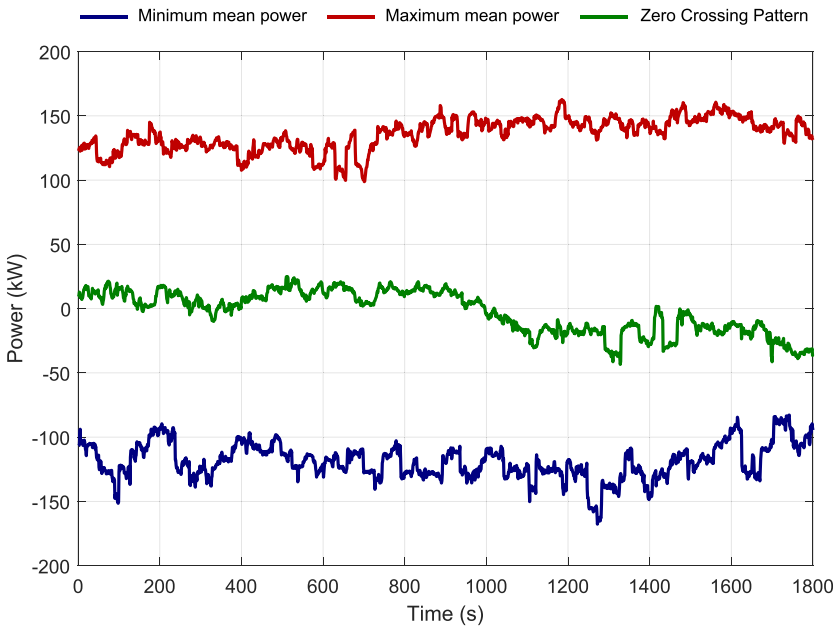

Fig. 6. Selected patterns of the input power profile. In detail, the profile with the maximum mean power is represented by the red line, while the profile corresponding to the minimum mean power is depicted by the blue line. The green line indicates the selected pattern corresponding to the case of power crossing zero. (For interpretation of the references to color in this figure legend, the reader is referred to the web version of this article.)

Table 3
BESS technical features for the considered simulation scenarios.

Parameter	Case 1: HESS Configuration	Case 2: non-hybrid Configuration
Chemistry	Nickel Manganese Cobalt oxide (NMC)	
Nominal Capacity	876 kWh	884 kWh
Max Dis-/charge Rate	0.15C	0.25C
Nominal Voltage	400 V	400 V
Operating voltage	300–420 V	300–420 V
Max DOC	90%	90%

Table 4
Daily cycles obtained by RFC application on LIB SoCs for non-hybrid and hybrid cases.

Cycle	Case 1 - HESS Li-ion Battery			Case 2 - Equivalent Li-ion Battery		
	$SoC_{init}(\%)$	$SoC_{fin}(\%)$	DoD	$SoC_{init}(\%)$	$SoC_{fin}(\%)$	DoD
1	50.0	58.7	+8.7	50.0	58.3	+8.3
2	58.7	58.2	−0.5	58.3	57.7	−0.6
3	58.2	58.4	+0.2	57.7	58.0	+0.3
4	58.4	19.0	−39.4	58.0	12.1	−45.9
5	19.0	100	+81.0	12.1	99.3	+87.2
6	100	43.0	−57.0	99.3	37.0	−62.3
7	43.0	43.3	+0.3	37.0	37.3	+0.3

Table 5
Step cycles for the accelerated test campaign on Li-ion cells in relation to Case 1 and Case 2.

Step	Case 1 - HESS Li-ion Battery			Case 2 - Equivalent Li-ion Battery		
	DoD	I_{cell} (A)	Time (s)	DoD	I_{cell} (A)	Time (s)
1	+8.7%	−4 ± 0.04	157	+8.3%	−4 ± 0.16	149
2	−0.5%	19.5 ± 0.04	2	−0.6%	19.5 ± 0.16	2
3	+0.2%	−4 ± 0.04	4	+0.3%	−4 ± 0.16	5
4	−39.4%	19.5 ± 0.04	142	−45.9%	19.5 ± 0.16	165
5	–	0	600	–	0	600
6	+81.0%	−4 ± 0.04	1458	+87.2%	−4 ± 0.16	1570
7	–	0	600	–	0	600
8	−57.0%	19.5 ± 0.04	205	−62.3%	19.5 ± 0.16	224
9	–	0	600	–	0	600
10	+0.3%	−4 ± 0.04	5	+0.3%	−4 ± 0.16	5

Table 6
Registered capacity values for the investigated cases.

Equivalent year	Case 1 - HESS Li-ion Battery	Case 2 - Equivalent Li-ion Battery
	Measured Capacity (mAh)	
0	2008.7	2013.8
1	1838.3	1804.7
2	1668.8	1622.0
3	1501.7	1302.9

6.1. Economic evaluation of HESS vs. BESS

To evaluate the cost-effectiveness of the standalone BESS and the HESS, the Levelized Cost of Storage (LCOS) [38,39] is computed over a 20-year operational lifetime [40].

The LCOS over 20 years is defined as:

$$\mathrm{LCOS}_{20y} = \frac{\sum_{t=1}^{20} \frac{C_{\mathrm{cap},t} + C_{\mathrm{O\&M},t}}{(1+r)^t}}{\sum_{t=1}^{20} \frac{E_t}{(1+r)^t}} \tag{14}$$

where $C_{\mathrm{cap},t}$ is the capital cost in year t (including battery replacements), $C_{\mathrm{O\&M},t}$ is the annual operating cost (assumed to be 2% of initial capital cost, based on the average values reported in the literature [41,42]), E_t is the discharged energy in year t, and r is the discount rate (7%) which reflects commonly used assumptions and averages from prior studies [43,44]. The cost parameters for the BESS and FESS, including both energy and power costs, are derived from the latest data provided in the PNNL report [41]. Due to the difficulty of precisely

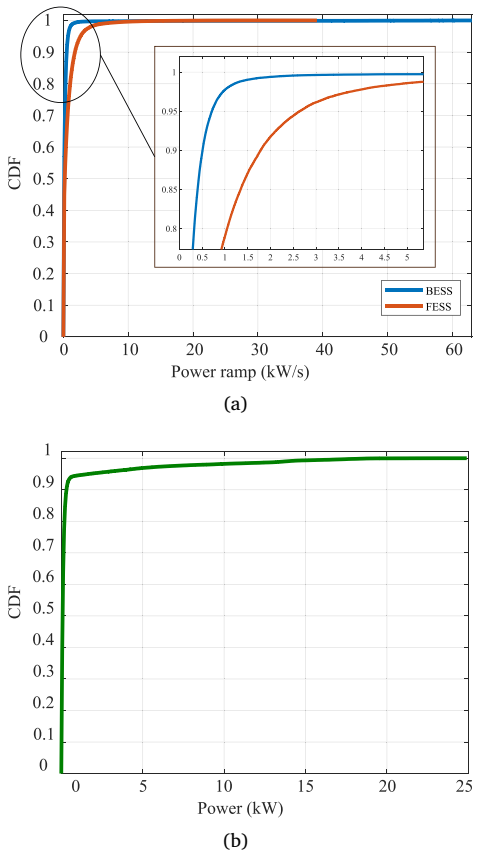

Fig. 7. (a) cumulative density functions of the BESS and FESS power ramps and (b) cumulative density function of the residual power not managed by HESS.

Table 7
Capital cost parameters for BESS and FESS.

Component	Power Cost (C_P) [$/kW]	Energy Cost (C_E) [$/kWh]
BESS	1446	362
FESS	1980	7920

Table 8
Power and Energy Ratings of Storage Systems.

Case	System	Power rating [kW]	Energy rating [kWh]	Total cost [$]
Case1: HESS	BESS	131.4	876	808080
	FESS	120	8	
Case2: Single BESS	BESS	221	884	639 574

estimating the capital cost, the total project cost is considered for this study. A detailed breakdown of these costs is presented in Table 7, and the system specification of each system and the corresponding total calculated cost are presented in Table 8. The total cost is calculated based on both the power cost C_P and energy cost C_E of each ESS as (15) [41,45].

$$\text{Total Cost}_{\text{ESS}} = C_P \cdot P_{\text{kW}} + C_E \cdot E_{\text{kWh}} \tag{15}$$

Battery replacement costs are assumed to match the original BESS unit cost. With efficiency of BESS being 90% and efficiency of FESS being 95% [46,47], the annual discharged energy for BESS is $E_{\text{BESS}} = 884 \cdot 365 \cdot 0.95 = 306{,}181$ kWh/year and for HESS is $E_{\text{HESS}} = (876 \cdot 0.95 + 8 \cdot 0.90) \cdot 365 = 306{,}381$ kWh/year.

Table 9
Replacement intervals for different SOH thresholds.

SoH Threshold [%]	BESS Interval [years]	BESS (HESS) Interval [years]	FESS Interval [years]
80	1.7	2.4	15
70	2.5	3.6	14
60	3.4	6.8	12
40	5.1	7.2	10

The determination of battery end-of-life thresholds in this study is based on the observed SoH degradation trends shown in Fig. 9(b) and summarized in Table 9. Different SoH thresholds (80%, 70%, 60%, and 40%) were considered to assess the sensitivity of battery replacement intervals on the LCOS [48,49]. The BESS replacement intervals were derived from experimental SoH degradation rates, while the FESS replacement intervals were assigned based on mechanical fatigue considerations. The time to reach each SoH threshold was calculated by dividing the usable SoH margin by the annual degradation rate for BESS, which allows a consistent estimation of replacement intervals under different degradation scenarios.

Unlike the battery, whose end-of-life is typically defined by a drop in SoH to a specified threshold, the flywheel's life in this study is governed primarily by mechanical fatigue of the composite rotor. Although bearing wear can be a major degradation mechanism in systems using conventional bearings, our FESS employs active magnetic bearings, which virtually eliminate contact-related wear and thereby extend bearing life considerably. The fatigue life of composite flywheel rotors is commonly reported between 10^8 to 10^9 equivalent cycles [50,51], depending on design and operational stresses. Considering the typical operating profiles in energy storage applications and accounting for mechanical stresses induced by deep torque cycles, a variable flywheel replacement schedule was adopted. Specifically, the FESS replacement interval was set to decrease progressively from 15 years to 10 years as cycling severity increased, corresponding to lower SoH thresholds. This approach reflects the increasing mechanical fatigue under more aggressive operational profiles, while maintaining realistic assumptions aligned with industrial practice.

The comprehensive comparison across these four cases is illustrated in Fig. 10, which reports the LCOS evolution over a 20-year horizon. The results demonstrate that HESS does not universally guarantee lower costs compared to standalone BESS configurations. Instead, the cost competitiveness of HESS strongly depends on the chosen SoH limit for battery end-of-life and the corresponding replacement timing. Specifically, in scenarios with stricter SoH thresholds (e.g., 80% and 70%), the HESS configuration often shows economic advantages due to the reduced battery cycling stress and extended battery lifespan. Conversely, for lower SoH thresholds (e.g., 60% and 40%), where batteries are replaced less frequently, the higher capital cost of integrating a flywheel becomes more pronounced, potentially offsetting the longevity benefits.

7. Conclusion

This study presents a comprehensive evaluation of a Hybrid Energy Storage System (HESS) composed of a lithium-ion battery and a flywheel, validated through experimental Power Hardware-in-the-Loop (PHIL) testing and long-term accelerated battery aging analysis. By combining dynamic modeling, real-time control implementation, and degradation-aware lifetime testing, the proposed framework provides an in-depth assessment of HESS performance under grid support scenarios. Specifically, the primary frequency regulation service to be provided to a micro-grid is considered the application case study.

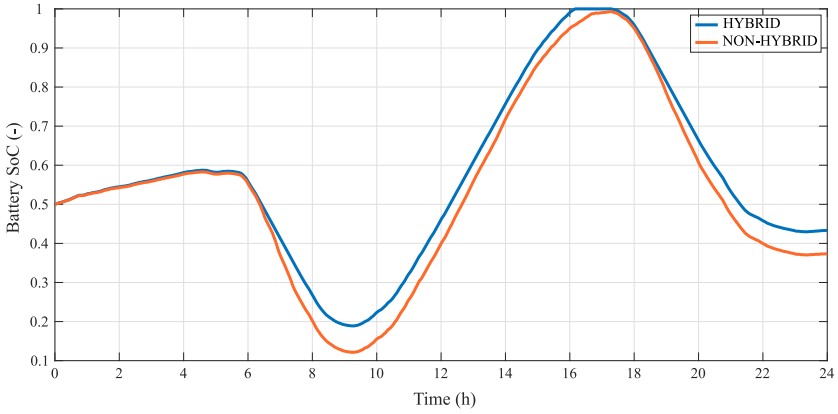

Fig. 8. BESS SoCs in case of hybrid (blue line) and non-hybrid (orange line) configurations. (For interpretation of the references to color in this figure legend, the reader is referred to the web version of this article.)

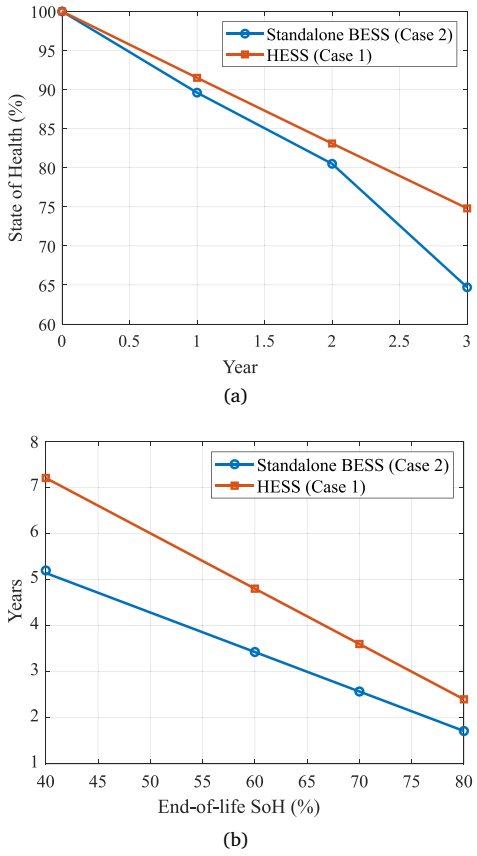

Fig. 9. (a) Measured State of Health (SoH) over time and (b) battery replacement timelines depending on SoH threshold.

The results demonstrate that HESS effectively reduces the power ramping burden and depth-of-discharge cycles on the battery, thereby extending its operational life compared to a standalone Battery Energy Storage System (BESS). Accelerated aging experiments confirmed 10% higher capacity retention in the HESS configuration after three equivalent years of operation.

Furthermore, a detailed Levelized Cost of Storage (LCOS) analysis over a 20-year horizon revealed that while HESS may not always offer lower costs than standalone BESS, it becomes increasingly cost-competitive under stricter battery end-of-life (SoH) thresholds due to reduced replacement frequency.

Future research will extend this study in several directions. First, the performance of the HESS will be evaluated under different power profiles and grid-support services, including scenarios involving deeper discharge cycles, to further investigate strategies that minimize the negative effects of unavoidable deep discharges on battery health. In addition, the PHIL framework developed in this work will be expanded to include a supercapacitor-based HESS configuration. This will enable a comparative assessment between flywheel and supercapacitor hybrid systems and their influence on the lifetime and performance of both lithium-ion and emerging sodium-ion batteries.

CRediT authorship contribution statement

Seyede Masoome Maroufi: Writing – review & editing, Writing – original draft, Visualization, Validation, Software, Methodology, Investigation, Formal analysis, Data curation, Conceptualization. **Dario Pelosi:** Writing – original draft, Validation, Methodology, Investigation. **Linda Barelli:** Writing – review & editing, Writing – original draft, Supervision, Methodology, Conceptualization. **Giovanni De Carne:** Writing – review & editing, Validation, Supervision, Resources, Project administration, Methodology, Formal analysis.

Declaration of Generative AI and AI-assisted technologies in the writing process

During the preparation of this work the authors used Grammarly in order to improve the English style of the manuscript. After using this tool, the authors reviewed and edited the content as needed and take full responsibility for the content of the publication.

Declaration of competing interest

The authors declare that they have no known competing financial interests or personal relationships that could have appeared to influence the work reported in this paper.

Acknowledgments

Masoome Seyede Maroufi and Giovanni De Carne are with the Institute for Technical Physics, Karlsruhe Institute of Technology, Germany. The work of Masoome Seyede Maroufi and Giovanni De Carne has been supported by the Helmholtz Association, Germany under the program “Energy System Design” and under the Helmholtz Young Investigator Group “Hybrid Networks” (VH-NG-1613).

Data availability

Data will be made available on request.

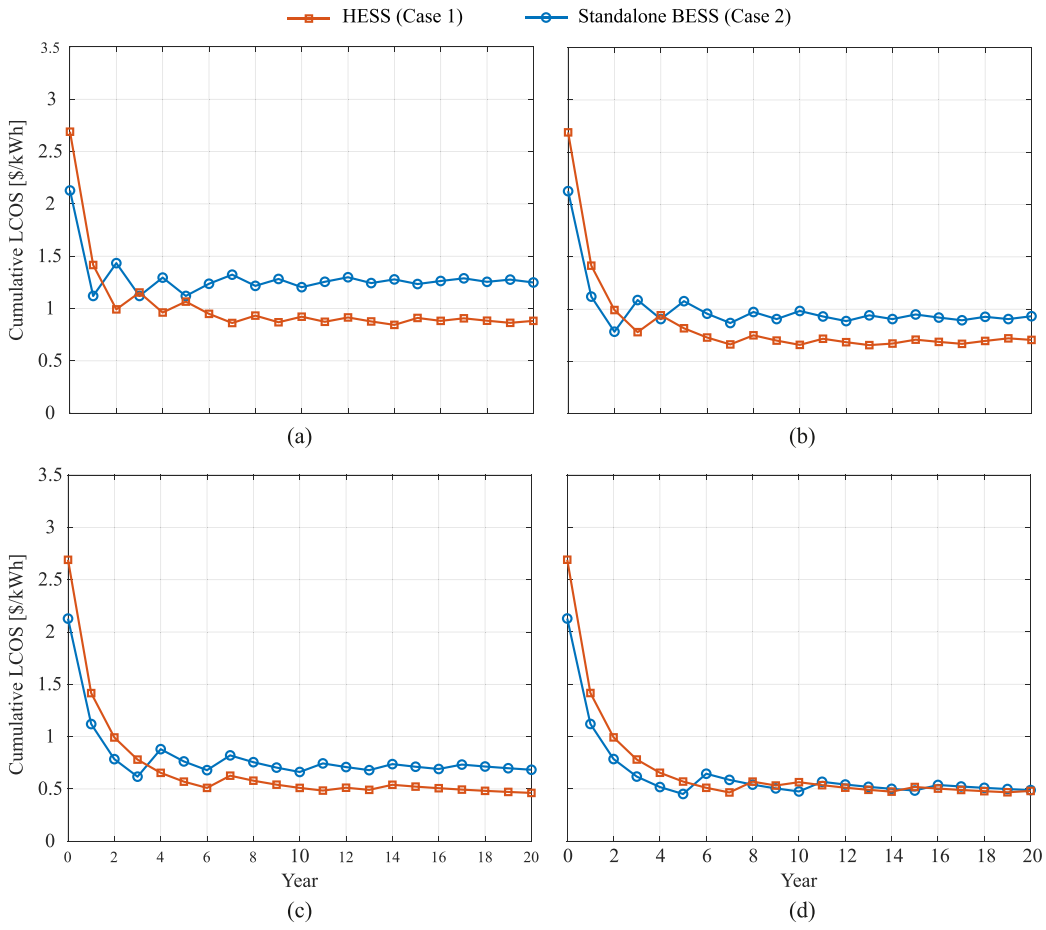

Fig. 10. Cumulative Levelized Cost of Storage (LCOS) over 20 years (a) replacement of the battery by 80% of SoH (b) replacement of the battery by 70% of SoH (c) replacement of the battery by 60% of SoH (d) replacement of the battery by 40% of SoH .

References

[1] C. Zhao, P.B. Andersen, C.T. holt, S. Hashemi, Grid-connected battery energy storage system: a review on application and integration, Renew. Sustain. Energy Rev. 182 (2023) 113400.

[2] G. De Carne, S.M. Maroufi, H. Beiranvand, V. De Angelis, S. D'Arco, V. Gevorgian, S. Waczowicz, B. Mather, M. Liserre, V. Hagenmeyer, The role of energy storage systems for a secure energy supply: A comprehensive review of system needs and technology solutions, Electr. Power Syst. Res. 236 (2024) 110963.

[3] R. Li, N.D. Kirkaldy, F.F. Oehler, M. Marinescu, G.J. Offer, S.E.J. O'Kane, The importance of degradation mode analysis in parameterising lifetime prediction models of lithium-ion battery degradation, Nat. Commun. 16 (1) (2025) 2776.

[4] A.M. Adeyinka, O.C. Esan, A.O. Ijaola, P.K. Farayibi, Advancements in hybrid energy storage systems for enhancing renewable energy-to-grid integration, Sustain. Energy Res. 11 (1) (2024) 26.

[5] D. Fusco, S. Masoome Maroufi, F. Porpora, M. Di Monaco, G. De Carne, G. Tomasso, Performance analysis of ASR-UKfs for supercapacitor SoC estimation in hybrid energy storage systems, IEEE J. Emerg. Sel. Top. Power Electron. 12 (6) (2024) 5602–5612.

[6] S.T. Sisakat, S.M. Barakati, Fuzzy energy management in electrical vehicles with different hybrid energy storage topologies, in: 4th Iranian Joint Congress on Fuzzy and Intelligent Systems, CFIS 2015, IEEE, 2016, pp. 10–15.

[7] T. Mesbahi, N. Rizoug, P. Bartholomeüs, R. Sadoun, F. Khenfri, P. Le Moigne, Optimal energy management for a li-ion battery/supercapacitor hybrid energy storage system based on a particle swarm optimization incorporating nelder–mead simplex approach, IEEE Trans. Intell. Veh. 2 (2) (2017) 99–110.

[8] S.M. Maroufi, G. De Carne, Optimal design for hybrid energy storage systems considering system aging and costs, in: 2023 IEEE 14th International Symposium on Power Electronics for Distributed Generation Systems, PEDG, 2023, pp. 496–500.

[9] K. Ding, F. Li, X. Zhang, Power Smoothing Control of DC Microgrid Hybrid Energy Storage System Based on Fuzzy Control, 2019, pp. 7296–7301.

[10] W. Yanzi, X. Changle, W. Wang, Energy management strategy based on fuzzy logic for a new hybrid battery-ultracapacitor energy storage system, IEEE Transp. Electrification Conf. Expo, ITEC Asia-Pacific 2014 - Conf. Proc. (2014) 1–5.

[11] O. Erdinc, B. Vural, M. Uzunoglu, A wavelet-fuzzy logic based energy management strategy for a fuel cell/battery/ultra-capacitor hybrid vehicular power system, J. Power Sources 194 (1) (2009) 369–380.

[12] S. Karrari, Integration of Flywheel Energy Storage Systems in Low Voltage Distribution Grids, KIT Scientific Publishing, 2023.

[13] K. Singh, M. Singh, S.K. Valluru, Ultracapacitor assisted battery based HESS for electric vehicle considering battery aging, IEEE J. Emerg. Sel. Top. Ind. Electron. (2025).

[14] M. Chen, Z. Liang, Z. Cheng, J. Zhao, Z. Tian, Optimal scheduling of FTPSS with PV and HESS considering the online degradation of battery capacity, IEEE Trans. Transp. Electrification 8 (1) (2021) 936–947.

[15] L. Lin, Y. Cao, X. Kong, Y. Lin, Y. Jia, Z. Zhang, Hybrid energy storage system control and capacity allocation considering battery state of charge self-recovery and capacity attenuation in wind farm, J. Energy Storage 75 (2024) 109693.

[16] S. Karrari, N. Ludwig, G. De Carne, M. Noe, Sizing of hybrid energy storage systems using recurring daily patterns, IEEE Trans. Smart Grid 13 (4) (2022) 3290–3300.

[17] S.M. Maroufi, S. Karrari, K. Rajashekaraiah, G. De Carne, Power management of hybrid flywheel-battery energy storage systems considering the state of charge and power ramp rate, IEEE Trans. Power Electron. 40 (7) (2025) 9944–9956.

[18] SAMSUNG SDI, Lithium-ion rechargeable cell for power tools model name: INR18650-20r, 2011, Technical datasheet.

[19] D. Pelosi, E. Castori, R. Aliberti, G. Marinelli, G. Sonnati, M. Marchetti, F. Rosignoli, N. Mulinari, L. Barelli, State of charge real-time evaluation of second-life batteries for islanded grid support, in: 2024 AEIT International Annual Conference, AEIT, 2024, pp. 01–05.

[20] L. Barelli, D.-A. Ciupageanu, A. Ottaviano, D. Pelosi, L. Gheorghe, Stochastic power management strategy for hybrid energy storage systems to enhance large scale wind energy integration, J. Energy Storage 31 (2020) 101650.

[21] L. Barelli, G. Bidini, D. Ciupageanu, A. Micangeli, P. Ottaviano, D. Pelosi, Real time power management strategy for hybrid energy storage systems coupled with variable energy sources in power smoothing applications, Energy Rep. 7 (2021) 2872–2882.

[22] A. Neffati, M. Guemri, S. Caux, M. Fadel, Energy management strategies for multi source systems, Electr. Power Syst. Res. 102 (2013) 42–49.
[23] R.H. Byrne, T.A. Nguyen, D.A. Copp, B.R. Chalamala, I. Gyuk, Energy management and optimization methods for grid energy storage systems, IEEE Access (2017) 1–1.
[24] L. Barelli, G. Bidini, D.A. Ciupageanu, A. Ottaviano, D. Pelosi, F. Gallorini, G. Alessandri, M. Atcheson Cruz, An effective solution to boost generation from waves: Benefits of a hybrid energy storage system integration to wave energy converter in grid-connected systems, Open Res. Eur. 2 (2022) 40.
[25] P. Sadegh, J. Spall, Optimal random perturbations for stochastic approximation using a simultaneous perturbation gradient approximation, IEEE Trans. Autom. Control 43 (10) (1998) 1480–1484.
[26] J. Spall, Overview of the simultaneous perturbation method for efficient optimization, 19, 1998, pp. 482–492, Hopkins APL Technical Digest.
[27] J.C. Spall, A one-measurement form of simultaneous perturbation stochastic approximation, Automatica 33 (1) (1997) 109–112.
[28] M. Ho, J. Lim, C.Y. Chong, K.K. Chua, A. Siah, High dimensional origin destination calibration using metamodel assisted simultaneous perturbation stochastic approximation, IEEE Trans. Intell. Transp. Syst. PP (2023) 1–10.
[29] O. Granichin, V. Erofeeva, Y. Ivanskiy, Y. Jiang, Simultaneous perturbation stochastic approximation-based consensus for tracking under unknown-but-bounded disturbances, IEEE Trans. Autom. Control 66 (8) (2021) 3710–3717.
[30] D.-A. Ciupageanu, L. Barelli, A. Ottaviano, D. Pelosi, G. Lazaroiu, Innovative power management of hybrid energy storage systems coupled to RES plants: The simultaneous perturbation stochastic approximation approach, in: 2019 IEEE PES Innovative Smart Grid Technologies Europe (ISGT-Europe), 2019, pp. 1–5.
[31] J. Spall, Multivariate stochastic approximation using a simultaneous perturbation gradient approximation, IEEE Trans. Autom. Control 37 (3) (1992) 332–341.
[32] J. Spall, Implementation of the simultaneous perturbation algorithm for stochastic optimization, IEEE Trans. Aerosp. Electron. Syst. 34 (3) (1998) 817–823.
[33] R. Siddaiah, R. Saini, A review on planning, configurations, modeling and optimization techniques of hybrid renewable energy systems for off grid applications, Renew. Sustain. Energy Rev. 58 (2016) 376–396.
[34] D. Pelosi, L. Barelli, A multi-objective Stochastic Power Management Strategy for Vehicle-to-Building and Building-to-Vehicle Integration into Residential Microgrids, 2023, pp. 1–6.
[35] D. Pelosi, F. Gallorini, G. Alessandri, L. Barelli, A hybrid energy storage system integrated with a wave energy converter: Data-driven stochastic power management for output power smoothing, Energies 17 (5) (2024).
[36] ASTM, E1049-85: Standard practices for cycle counting in fatigue analysis, 2011, E1049 - 85, 1–10.
[37] K.-H. Chang, G. Lin, Optimal design of hybrid renewable energy systems using simulation optimization, Simul. Model. Pr. Theory 52 (2015).
[38] P.G. Anselma, P.J. Kollmeyer, S. Feraco, A. Bonfitto, G. Belingardi, A. Emadi, N. Amati, A. Tonoli, Economic payback time of battery pack replacement for hybrid and plug-in hybrid electric vehicles, IEEE Trans. Transp. Electrification 9 (1) (2023) 1021–1033.
[39] S. Atalay, M. Sheikh, A. Mariani, Y. Merla, E. Bower, W.D. Widanage, Theory of battery ageing in a lithium-ion battery: Capacity fade, nonlinear ageing and lifetime prediction, J. Power Sources 478 (2020) 229026.
[40] O. Schmidt, S. Melchior, A. Hawkes, I. Staffell, Projecting the future levelized cost of electricity storage technologies, Joule 3 (1) (2019) 81–100.
[41] K. Mongird, V.V. Viswanathan, P.J. Balducci, M.J.E. Alam, V. Fotedar, V.S. Koritarov, et al., Energy Storage Technology and Cost Characterization Report, Technical Report, Pacific Northwest National Laboratory (PNNL), Richland, WA, United States, 2020, (Accessed 16 May 2020).
[42] V. Jülch, Comparison of electricity storage options using levelized cost of storage (LCOS) method, Appl. Energy 183 (2016) 1594–1606.
[43] B. Zakeri, S. Syri, Electrical energy storage systems: A comparative life cycle cost analysis, Renew. Sustain. Energy Rev 42 (2015) (2015) 569–596.
[44] J.M. Eyer, Benefits from flywheel energy storage for area regulation in California-demonstration results: a study for the DOE Energy Storage Systems program, Technical Report, Sandia National Laboratories (SNL), Albuquerque, NM, and Livermore, CA ..., 2009.
[45] U.S. Department of Energy, Office of Electricity and Energy Reliability, Energy storage technology and cost characterization report, Technical Report PNNL-29766, Pacific Northwest National Laboratory (PNNL), 2019, (Accessed 20 June 2025).
[46] X. Hu, C. Zou, C. Zhang, Y. Li, Technological developments in batteries: A survey of principal roles, types, and management needs, IEEE Power Energy Mag. 15 (5) (2017) 20–31.
[47] M.E. Amiryar, K.R. Pullen, D. Nankoo, Development of a high-fidelity model for an electrically driven energy storage flywheel suitable for small scale residential applications, Appl. Sci. 8 (3) (2018).
[48] E. Martinez-Laserna, E. Sarasketa-Zabala, I. Villarreal Sarria, D.-I. Stroe, M. Swierczynski, A. Warnecke, J.-M. Timmermans, S. Goutam, N. Omar, P. Rodriguez, Technical viability of battery second life: A study from the ageing perspective, IEEE Trans. Ind. Appl. 54 (3) (2018) 2703–2713.
[49] M. Shahjalal, P.K. Roy, T. Shams, A. Fly, J.I. Chowdhury, M.R. Ahmed, K. Liu, A review on second-life of li-ion batteries: prospects, challenges, and issues, Energy 241 (2022) 122881.
[50] R. Sebastián, R. Peña Alzola, Flywheel energy storage systems: Review and simulation for an isolated wind power system, Renew. Sustain. Energy Rev. 16 (9) (2012) 6803–6813.
[51] C. Mc Nelis, S. Dunleavy, D. Stenzel, S. Cummins, Design and development of a large scale flywheel energy storage system (Ph.D. thesis), 2022.